26. Boore, D. M., *Bull. Seismol. Soc. Am.*, 1983, **73**, 1865–1894.
27 Kanai, K., *Bull Earthquake Res. Inst*, University of Tokyo, 1957, **35**, 309–325.
28 Vanmarcke, E. H., in *Seismic Risk and Engineering Decisions*, (eds. Lomnitz, C. and Rosenblueth, E.), Elsevier, Amsterdam, 1977, pp. 287–337.
29. Iyengar, R. N. and Iyengar, K. T. S. R., A nonstationary random process model for earthquakes and its application. Structures Research Report I/69, Dept. of Civil Engg., IISc., Bangalore, 1969.
30. Jennings, P. C., Housner, G. W. and Tsai, N. C., Proc. 4th WCEE, 1969, pp 145–160
31. Penzien, J. and Watabe, M., *Earthquake Engg. Struct. Dyn.*, 1975, **3**, 365–373.
32. Hadjian, A H., *Bull. Seismol. Soc. Am.*, 1981, **71**, 1323–1331.
33. Levy, R. F. Kozin and Moorman, R. B. B, *J. Engg. Mech. Div. Proc. ASCE*, 1971, **97**, 495–517.
34 Hsu, T.-I. and Bernard, M. C., *Earthquake Engg. Struct. Dyn.*, 1978, 347–362.
35. Schiff, A. and Bogdanoff, J. L., *Some Problems in Engineering Seismology*, Centre for Applied Stochastics, Purdue University, 1966.
36. Nau, *et al.*, *Bull. Seismol. Soc. Am.*, 1982, **72**(2), 615–636.
37. Cartwright, D. E. and Longuet-Higgins, M. S, Proc. Roy. Soc. London, 1956, **A237**, 212–232.
38. Newmark, N. M. and Rosenblueth, E., eds. *Fundamentals of Earthquake Engineering*, Englewood Cliffs, N. J. Prentice-Hall, 1971.
39. Trifunac, M. D., *Bull. Seismol. Soc. Am.*, 1971a, **61**(6), 1739–1753.

Seismic hazard estimation using modelling of earthquake strong ground motions: A brief analysis of 1991 Uttarkashi earthquake, Himalaya and prognostication for a great earthquake in the region

K. N. Khattri*, G. Yu†, J. G. Anderson†, J. N. Brune† and Y. Zeng†
*Wadia Institute of Himalayan Geology, Dehradun 248 001, India
†Seismological Laboratory and Department of Geological Sciences, Mackay School of Mines, University of Nevada, Reno, Nevada 89557, USA

The highly random like strong motions from earthquakes are modelled by representing the earthquake rupture as a superposition of subevents occurring randomly on the fault plane. The shapes of these subevents are assumed to be circular and their sizes are governed by a power law satisfied by self-similar processes. A composite source-time function is constructed by superposition of the individual time functions which are taken to be Brune pulses commensurate with the corresponding moments, stress drops, and corner frequencies for the subevents. Green's functions are calculated for the appropriate fault plane solution, velocity structure, and source station distances, and convolved with the composite source time function to obain the strong motion time history at a site. We present models of a couple of strong motion accelerograms of the 1991 Uttarkashi earthquake to demonstrate the usefulness of this method and its promise of generating strong motion histories of future earthquakes, thereby providing a sharper approach to seismic hazard assessment.

THE usual characterization of earthquake hazard using single parameter representation such as the peak ground acceleration is found inadequate for the safe design of many critical structures, thereby spurring a continual search for more suitable methods for estimating strong ground motion time histories for future earthquakes that would provide a holistic description of seismic hazard. Since records of strong motion accelerograms are not plentiful, one of the methods used is to scale one of the existing strong motion accelerograms for the appropriate magnitude and distance. However, this method has limitations as it is unable to take into account appropriate site conditions, focal mechanisms, variability in the complexity of earthquake source processes, etc.

Since the strong motion accelerograms display considerable randomness, a stochastic model, known as the 'and ω-squared model' has been developed in which the strong ground motion accelerograms are represented by random noise whose spectrum is band limited between the corner frequency f_0 and the high cut frequency f_{max}[1–3]. The spectral shape in the pass band is specified by Brune[4,5] spectrum parameterized by seismic moment M_0 and the attendant stress drop of the earthquake. The limitations of this approach are that it does not relate to physics of the process and therefore does not generate three-component accelerograms with expected coherency, phases of arrivals like P waves; besides dispersed surface

waves are not included, i e. the spectrum is not adequately modelled.

In another method, the use of observed seismograms of small earthquakes (empirical Green's functions) for obtaining accelerograms for a large earthquake has been shown to be a promising approach[1, 3, 6, 7]. The difficulties associated with this method are that the empirical Green's functions may not be available for appropriate source mechanism for the large earthquake, and for appropriate source site distance. Further the signal-to-noise ratios at lower frequencies may not be adequate.

Deterministic kinematic source models have also been used for synthesizing strong ground motions produced by earthquakes. These employ convolution of the slip function over the fault plane with Green's function for the appropriate earth model[3, 8]. The impediments in this method arise on account of inadequately representing the complexity of faulting process as well as inadequacy of the synthetic Green's functions at high frequencies due to complexities of the earth structure.

In this paper we present an application of a composite source model that takes into account the random nature of the complex source slip function which together with the use of synthetic Green's functions enables simulation of realistic accelerograms of earthquakes[9].

The complex source model

The heterogeneities in the rocks due to composition and geometrical structures cause rupture in a faulting process to be highly irregular. The effect of this is especially seen at higher frequencies. In order to model the rupture phenomena Zeng *et al.*[9] developed the complex source model in which the main earthquake faulting is represented by a large number of subevents which are randomly distributed over the fault plane of the main earthquake. The subevents are taken to be circular in shape. The radius of these subevents is governed by constraint of self-similarity[10]. The rupture is started at the nucleation point and propagates at constant velocity to cover the entire area of the main fault. As the rupture front touches the centre of a particular subevent, it radiates a source pulse given by[8]:

$$s_i(t) = (R_{\theta\phi}\, w_c^2/4\pi\rho\, v_s^3)\, \dot{M}'_0\, t' \exp\{(-w_c t')\, H(t')\}, \quad (1)$$

where $R_{\theta\phi}$ is the radiation pattern, ρ the density, v_s the shear wave velocity, r the source to station distance, w_c the corner frequency, $t' = t - r/v_s$, M'_0 is the seismic moment of the i th subevent, and $H(.)$ is the unit step function. In defining the source pulse it has been assumed that the time function is given by the Brune[4, 5] pulse. The radius of the subevent, the stress drop and its seismic moment are related by[11]:

$$M_0(R) = (16/7)\, R_i^3\, \Delta\sigma \quad (2)$$

and the corner frequency by the following relation[4, 5].

$$w_0 = 2.34\, v_s/(2\pi R). \quad (3)$$

The seismic moment M_0 of the main event is obtained by summing the seismic moments of the subevents.

$$M_0 = \sum_{i=1}^{N} M'_0 = (16/7)\, \Delta\sigma \sum_{i=1}^{N} R_i^3, \quad (4)$$

where N is the total number of subevents. The stress parameter is adjusted in simulations to achieve the above equality. This adjustment is usually less than 10%[9].

The subevents are distributed over the designated fault plane randomly. They are allowed to overlap. However, the centres of the subevents are not allowed to fall outside the fault plane. Thus the total area covered by the subevents may be greater than the area of the fault plane. The number of events with radius R or greater is given by the following expression[9]:

$$N(R) = (p/D)\, R_{\text{main}}^D\, [R^{-D} - R_{\max}^{-D}]. \quad (5)$$

In the above equation $R_{\max}$ is permitted to be different from R_{main} but in the present analysis they are approximately equal. D is the fractal dimension, p is a constant of proportionality. It is determined by the constraint that the sum of seismic moments of subevents equals the target earthquake seismic moment. Thus using the relation:

$$M_0 = \int_{R_{\min}}^{R_{\max}} M_0(R)\, (-\mathrm{d}N/\mathrm{d}R)\, \mathrm{d}R, \quad (6)$$

one obtains

$$p = [7M_0\,(3-D)]/[16\Delta\sigma R_{\text{main}}^D\, (R_{\max}^{(3-D)} - R_{\min}^{(3-D)})];$$
$$D \neq 3, \quad p = (7M_0)/[16\Delta\sigma\, R_{\text{main}}^3\, \ln(R_{\max}/R_{\min})]; \; D = 3. \quad (7)$$

The numerical constraints define the parameter $R_{\min}$. The value of p is generally insensitive to its choice in the case of $D = 2$.

According to Frankel[10], the displacement spectrum from the above model of rupture will decay at high frequencies as $\omega^{(D/2-3)}$ provided the stress drop $\Delta\sigma$ is the same for all the subevents.

The sizes of the subevents are obtained by generating N random real numbers, N_i, which are uniformly distributed from 0 to N. The radius of the subevent corresponding to N_i is given by:

$$R_i = [DN_i/(pR_{main}^D) + R_{max}^{-D}]^{-1/D}. \quad (8)$$

An example of size distribution obtained in the above manner for $R_{max} = 20$ km, $R_{main} = 40$ km and $D = 2$ is shown in Figure 1. Figure 2 shows an example of 10% of all subevents that are used to generate an earthquake.

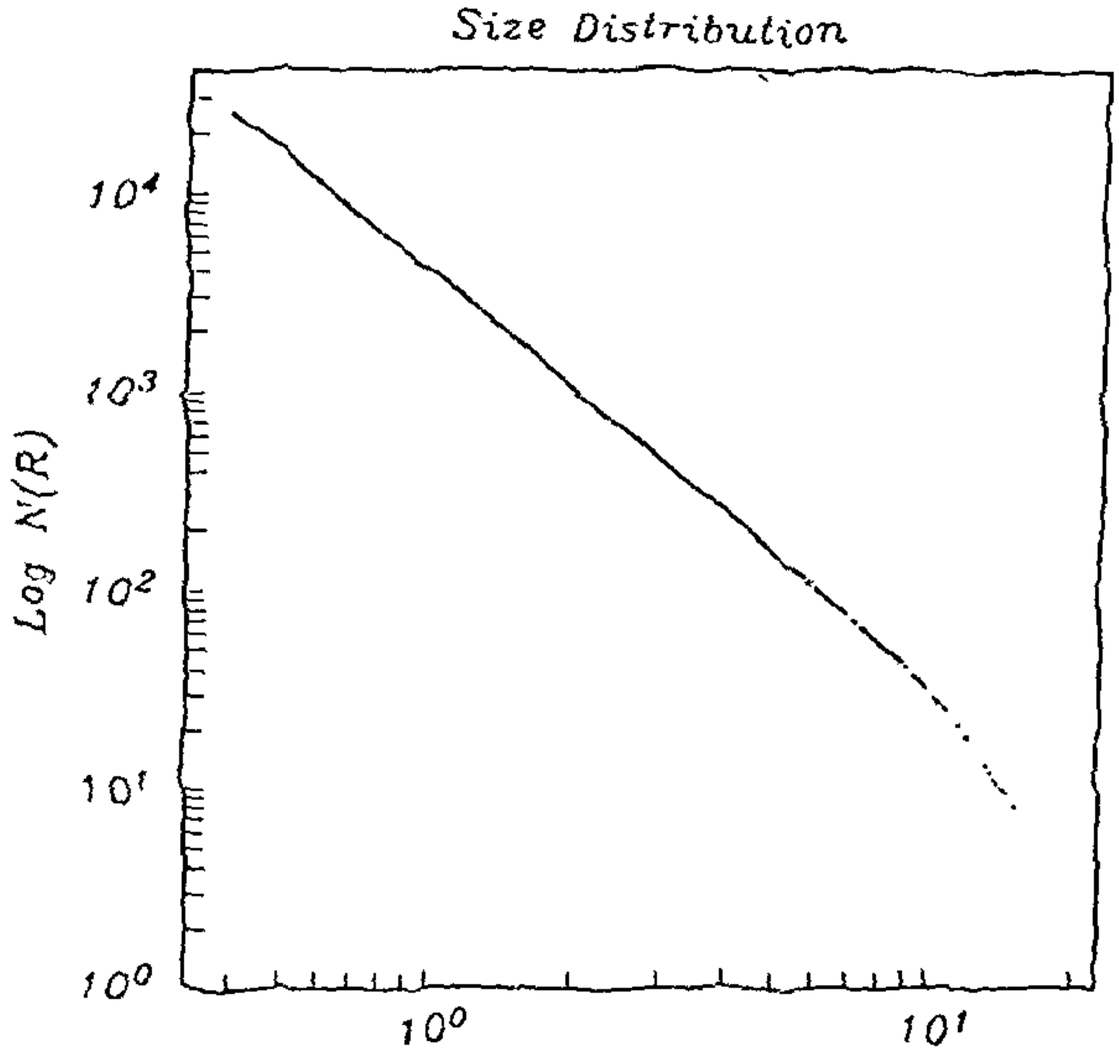

Figure 1. Distribution of sizes of subevents realized in a simulation for the case of $R_{max} = 20$ km, $R_{main} = 40$ km, and $D = 2$. After Zeng *et al*[9].

The source time function is calculated for the composite source model by superposing the source pulse for each subevent which is delayed with respect to the one at the hypocentre by the sum of rupture time and the travel time delay for S phase from the event to the station with respect to the hypocentre.

Since the number of subevents is very large, it is not computationally efficient to calculate the Green's function for each of them independently. Instead we divide the fault plane into approximately a square grid. For each of these grids a Green's function is calculated as also a composite source time function. These are convolved and the resulting ground motions for all the elements of the grid are summed to give the strong ground motion seismogram at the site.

The Green's functions are synthesized for a plane layered earth model using the wave number integration method[12].

The Uttarkashi earthquake

The magnitude M_s 7.0 Uttarkashi earthquake occurred in the Garhwal Himalaya and caused considerable loss of life and economic damage. The earthquake was located just north of the Main Central Thrust (MCT) in the crystalline terrane (Figure 3). A 260 m high dam is under construction at Tehri which is about 50 km to the south of the earthquake epicentral zone, in the Lesser

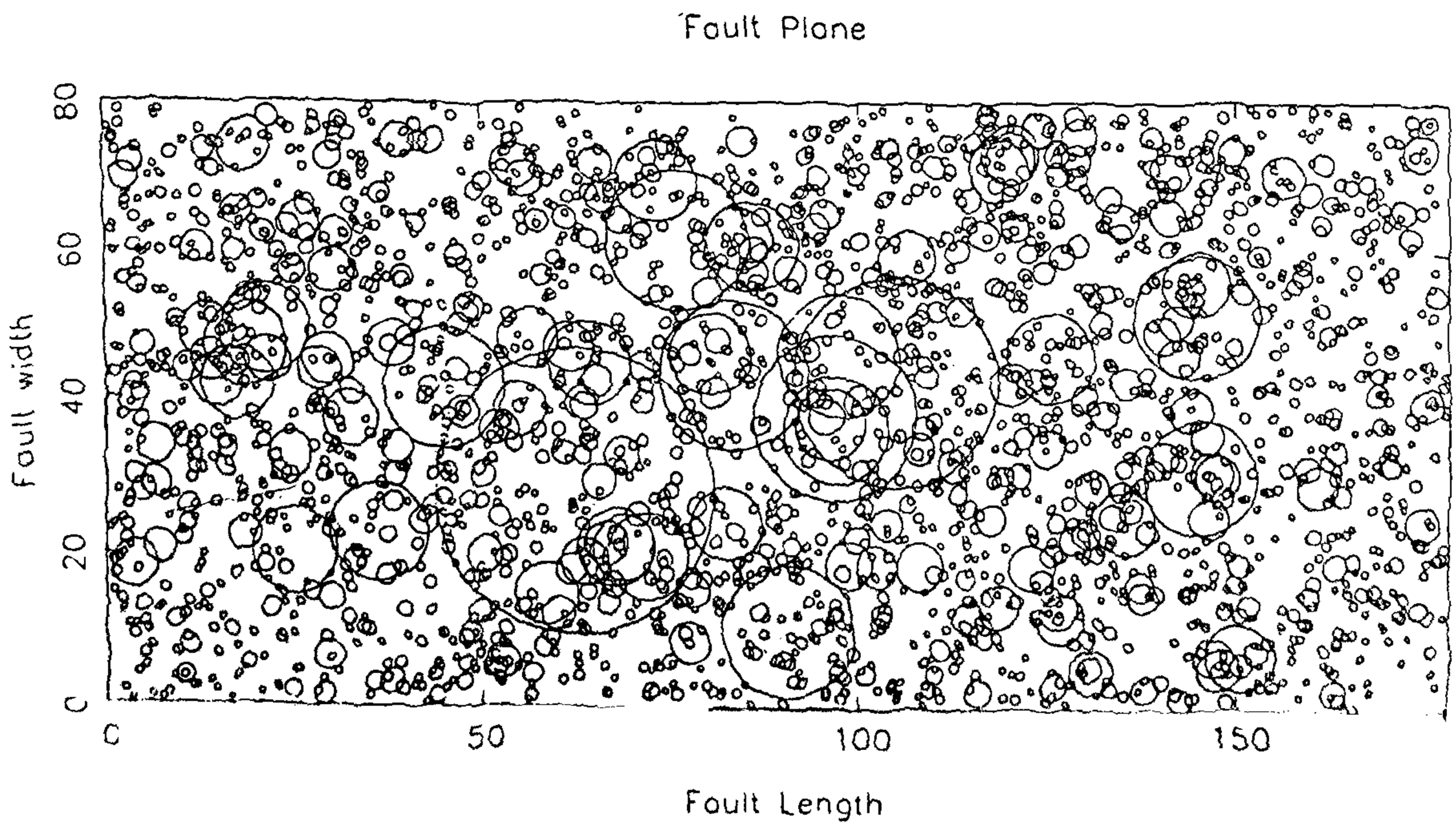

Figure 2. Ten per cent of the subevents obtained in the case of one simulation to represent one earthquake. After Zeng *et al*[9].

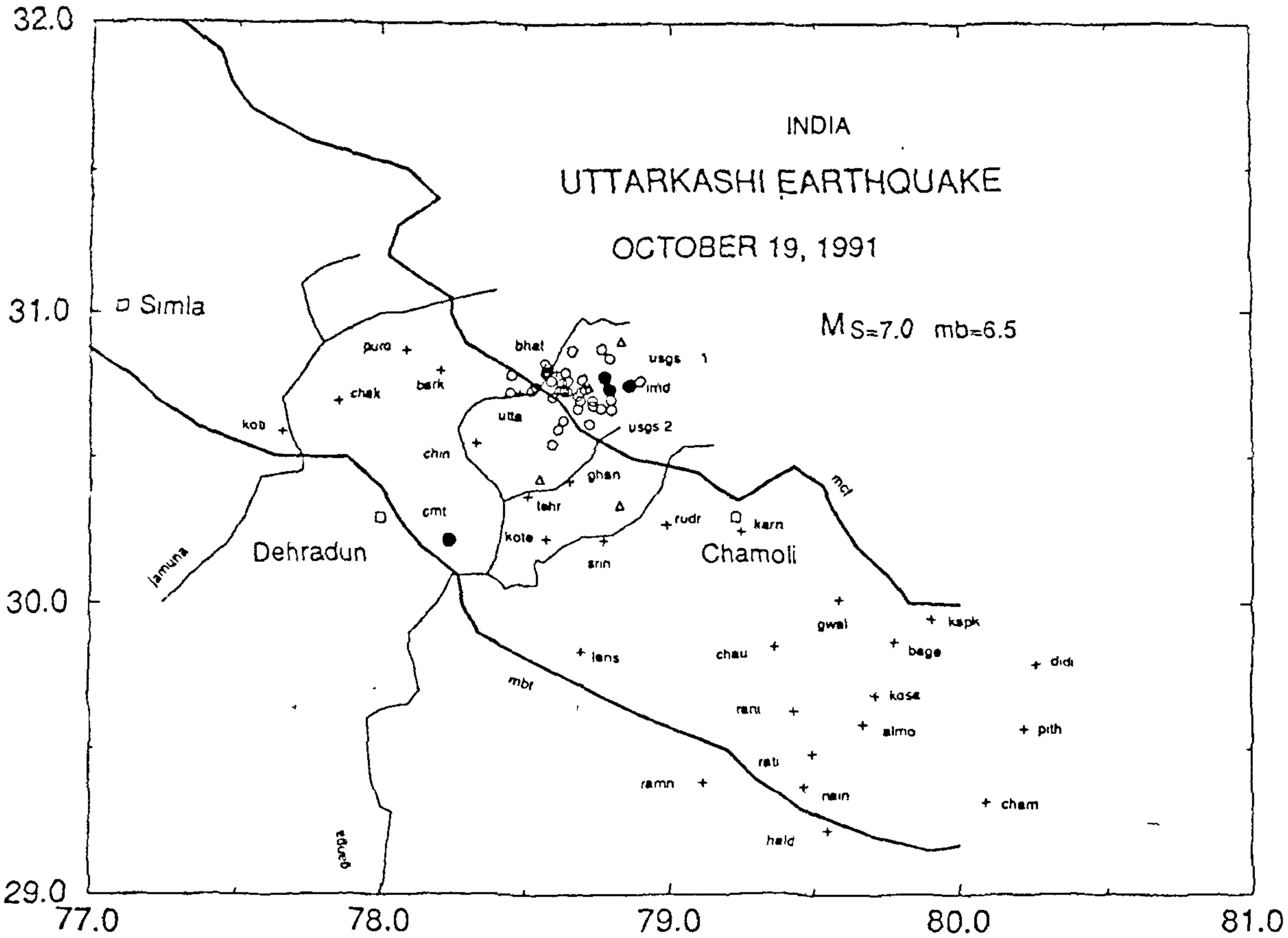

Figure 3. Locations of 1991 Uttarkashi main shock, some aftershocks, strong motion recording sites, and locations of Main Central Thrust, Main Boundary Thrust, main rivers, and towns. The open circles depict aftershocks located by local network, triangles are aftershocks reported by PDE.

Himalaya.. The following estimates of earthquake parameters have been used in the present study:

Hypocentral parameters: Lat: 30.75 N, Long: 78.86 E, H: 12 km (IMD); ot: 21 : 23 : 14.3 GMT; 19.10.1991
M_s: 7.0; m_b: 6.5; M_w: 6.8; M_0: 1.8×10^{26} dyne-cm (PDE, monthly, October 1991).

Fault plane solution:

NP1: strike 317°, dip 14°, slip 115°
NP2: strike 112°, dip 78°, slip 84°

Thus both the nodal planes of the earthquake have a strike nearly parallel to the local strike of the MCT. The north east dipping nodal plane is consistent with the model of underthrusting from the south in the Himalaya and is the preferred fault plane.

Several aftershocks were recorded by a local seismic network and these are also shown in Figure 3. They approximately define the outline of the fault plane. A few aftershocks were located by global network and are shown in the same figure. These appear to be more widely scattered around the epicentral zone perhaps because they may have relatively inferior accuracy.

The earthquake was recorded by 13 stations of a 28-station strong motion accelerograph network[13]. The network locations are shown in Figure 3. It is noted that all the stations except BHAT and UTTA lie on the southern side of the epicentral zone. The two sites mentioned above are at the western edge of the epicentral zone (fault plane). Also the station at BHAT is the only station located in the crystalline province of Great Himalaya north of MCT, the rest are located in the metasedimentary province of Lesser Himalaya on the south of the MCT.

Three-component analog recordings of strong motion were made using SMA-1 accelerographs. These were digitized and processed to obtain filtered digital ground

acceleration time histories at a sampling interval of 0.02 s. An Ormsby filter with characteristics (0.17, 0.20; 25.0, 27.0 Hz) was applied. This data had been obtained from Prof. A. R. Chandrasekaran through the Department of Science and Technology. This earthquake was investigated in detail by Yu *et al.*[14]. We briefly discuss here some of their results and comment on their implications to seismic hazard assessment.

The earthquake rupture is represented by a fault plane (NP1) dipping gently to the northeast at 14° with a dimension of 16 × 24 km. The dimension was constrained by empirical relation between magnitude and fault area as well as by the reported distribution of aftershocks of this earthquake. This model fault was divided into four 8 × 12 km elements for calculating the respective composite source time functions and synthetic Green's functions for ultimate summation to give the strong motion time histories at various sites. The values of other parameters were chosen to be: $D = 2$, $\Delta\sigma = 30$ bars, $R_{max} = 8$ km, and $v_r = 2.7$ km/s. The site at Bhatwari located in a higher region of Himalaya, is expected to have a near-surface zone comprising of decompressed rock of diminished velocities. Therefore a velocity model for this site was adopted from Khattri[15] by including a couple of layers at the top having lower velocities and Q. The model is shown in Table 1. The synthesized strong ground motions as well as the observed ones are shown in Figure 4. The synthetics were calculated up to 10 Hz only to economize on computer time. The synthetics have been band pass-filtered with the same frequency cut-off as the observed data. The observed ground motions are shown on the left and the synthetics on the right. The dashed lines show the observed and the continuous lines the synthetic spectrum.

The appearance of the synthetics is qualitatively quite similar to observed ground motion time histories. The match appears to become better for velocity and displacement time histories. The peak acceleration amplitudes are within a factor of 2 to 3 of the observed values. The overall spectral contents also match, with the best match for L component. In the V component there is greater energy in the band of 2–5 Hz and in the T component the synthetics have greater energy in frequencies above 4 Hz.

We note that the amplitudes of the envelopes of observed accelerograms for the three components have less variation between them than in the case of synthetics where the T component is largest and the V component is smallest. This and other variations may partly be accounted for by diffraction associated with heterogeneities of the medium which has not been modelled here, the imprecise and partial knowledge of even the layered earth velocity and Q structures used, in particular for the near surface at the site, and the source model in which the radiations at high frequencies from the rupture front have not been specifically modelled. Some of these effects may cause a quasi-homogenization of the amplitudes of the observed strong ground motions.

Since the synthetic accelerograms are governed by the composite source time functions, a number of realizations for the subevent distribution have been tried to investigate the stability of results. Ten such simulations are shown for one component in Figure 5. All the ten simulations are consistent in terms of appearance, duration, and amplitude within small variations. The method appears to be stable. The variability found in the above simulations may prove to be an advantage in modelling ground motions for some future earthquakes, as one may use a large number of such simulations in order to derive a distribution of various representative parameters of strong ground motion or find average predicted accelerograms with associated standard deviations. Possible variations in strong motion time histories due to variations in source models, for example, fault plane solutions, stress drops, etc. could also be investigated statistically in a similar manner.

The model for Tehri strong ground motions is shown in Figure 6. For this, the earlier velocity model was modified by trial and error to take into account the fact that this station is located in Lesser Himalaya comprising of metasedimentary formations. It is noted that a detailed knowledge of velocity and Q structures are not available for any of the sites of the strong motion stations in Himalaya. The velocity structure obtained after some trial and error is given in Table 2. The resulting synthetics in general are richer in higher frequencies. Thus, they are more energetic for longer durations. The peak amplitudes are comparable. The low amplitude of L component is a nodal plane effect. A better knowledge of the shallow site velocity and Q structures would be helpful in investigating whether an improved fit could be obtained through its use. For example the observed spectrum displays a broad minimum at around 2 Hz which may be due to local site velocity structure. The spectrum also displays peaking and an enrichment of energy between 1 and 2 s. Such a peaking is not present at Bhatwari. It could be a valley resonance effect[16]. Such aspects need further investigation.

Pseudo-relative response spectra at Bhatwari and Tehri

Table 1. Reference regional velocity model

Thickness (km)	V_p (km/s)	Q_p	V_s (km/s)	Q_s	Density (g/cm^3)
0 4	3 5	50	2 00	25	1 80
1 0	5 0	80	2 86	50	2 40
15 0	5 2	4000	2 97	2000	2 60
30 00	6 0	4000	3 43	2000	2 90
Infinity	8 33	1000	4 83	500	3.30

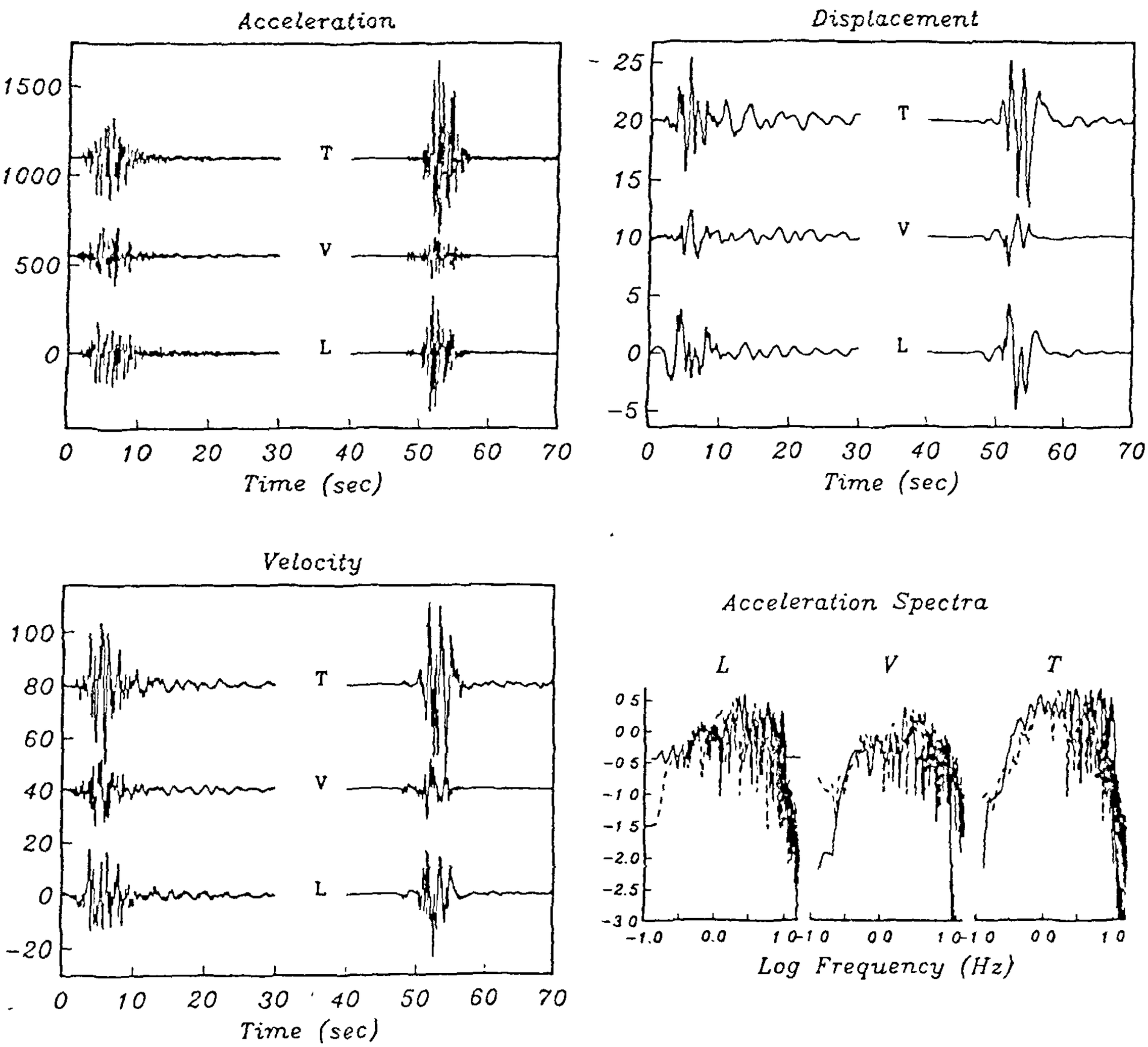

Figure 4. Comparison of observed and synthetic ground motions at Bhatwari for the 1991 Uttarkashi earthquake. Observed time histories are on the left and simulated are on the right. The dashes represent the observed spectrum and continuous lines the simulated spectrum After Yu *et al.*[14].

respectively are displayed in Figures 7 and 8. The solid lines having smaller amplitudes are the empirical responses to the digitized accelerograms recorded for the Uttarkashi earthquake. The response spectra for synthetic accelerograms for Uttarkashi earthquake model are shown by short dash lines for the case of no filtering and by long dash lines for the case of filtering corresponding to the filters used in data processing of observed seismograms. The filtered response is consistent with that recorded at Bhatwari, but at Tehri the response for the synthetic case is deficient in energy in the period band 1–4 s as also noted above. On the other hand, the response spectra at both the stations corresponding to unfiltered synthetics have a much larger amplitude at low frequencies. The energy at low frequencies in the observed accelerograms is likely to have been filtered out in the process of data preparation.

The above results as also those obtained by Zeng

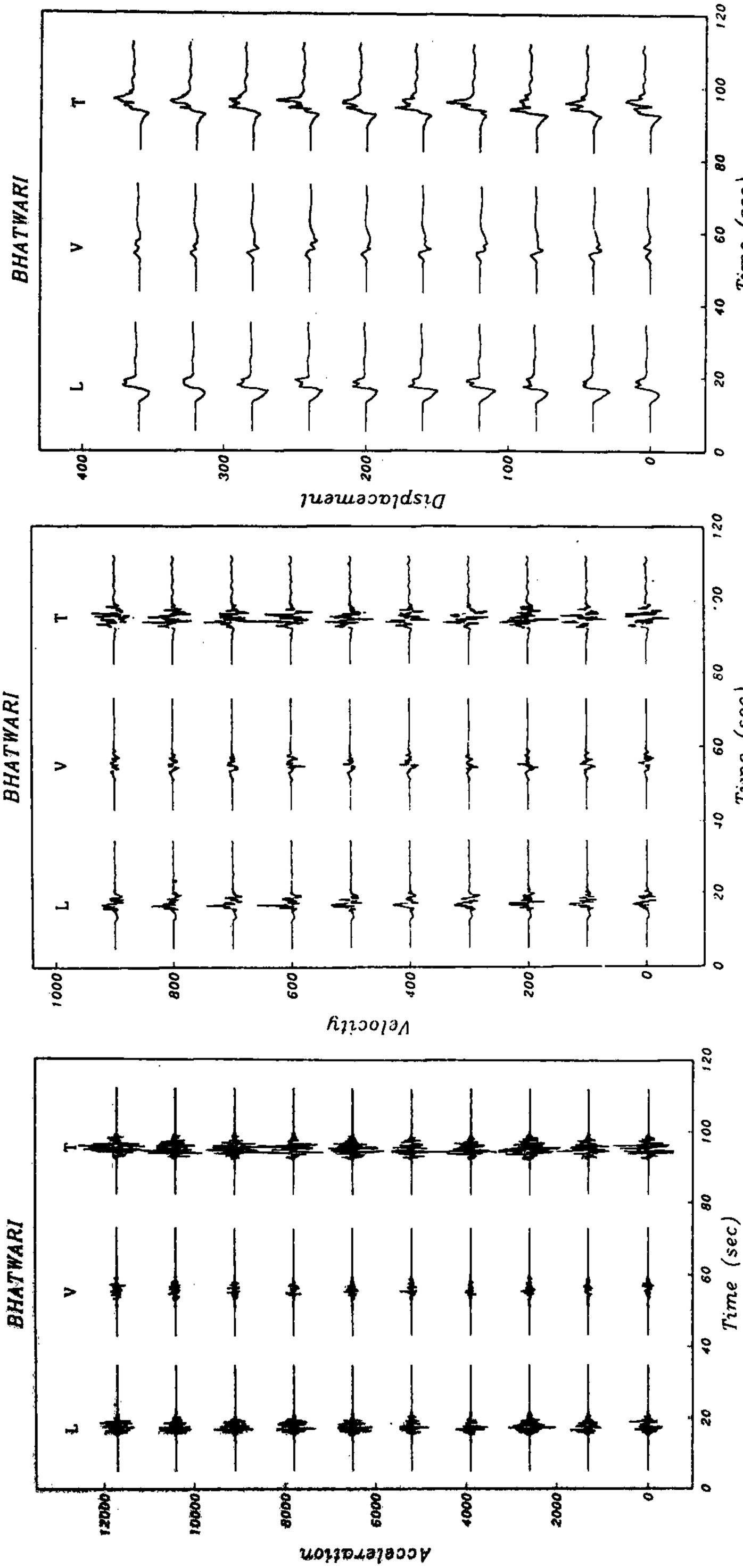

Figure 5. Multiple realizations of synthetic accelerations, velocity, and displacement time histories for one component at Bhatwari. After Yu *et al.*[14].

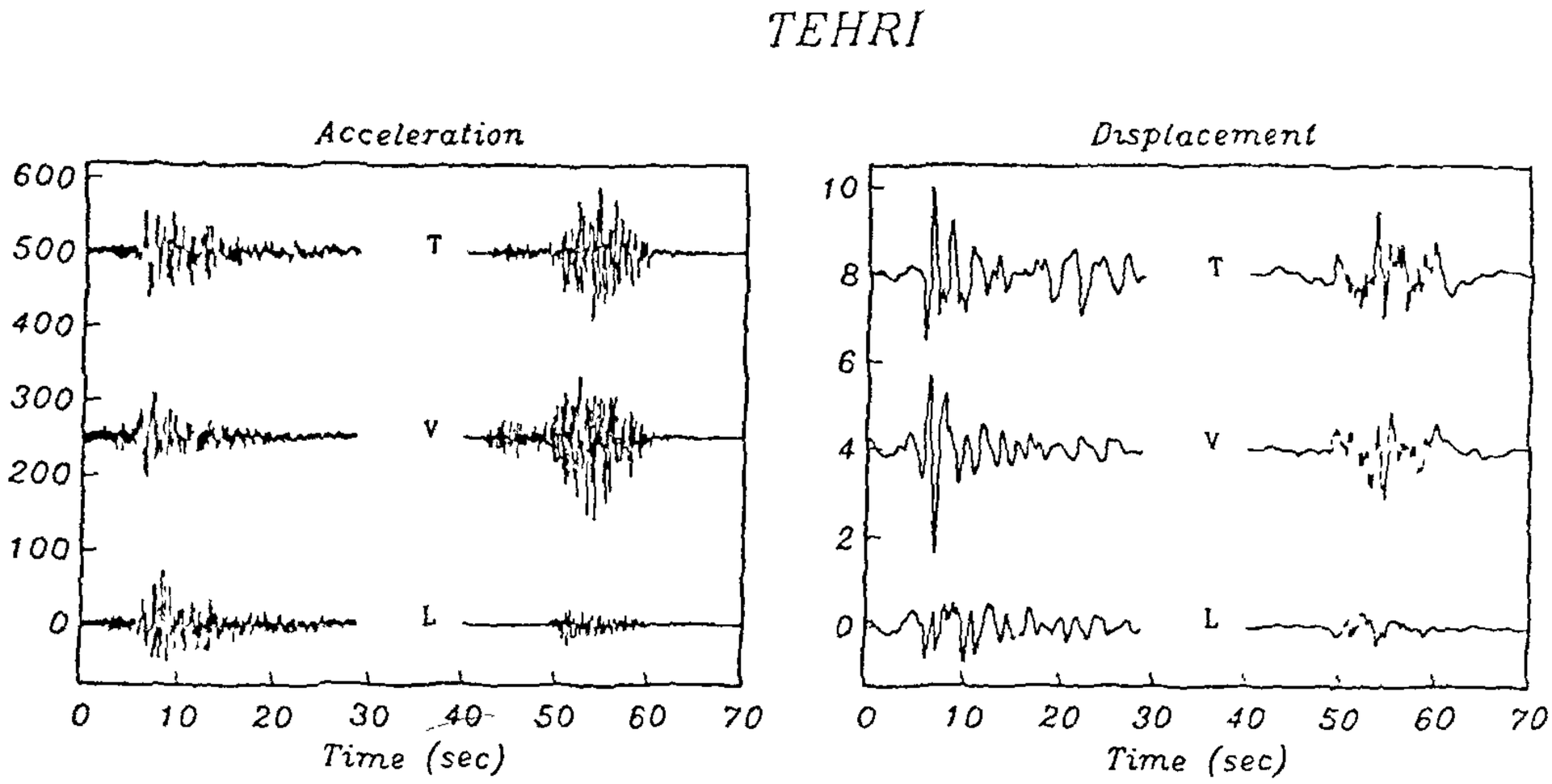

Figure 6. Observed and synthetic ground motions for Tehri for the 1991 Uttarkashi earthquake. After Yu *et al.*[14].

Table 2. Velocity model for Tehri region

Thickness (km)	V_p (km/s)	Q_p	V_s (km/s)	Q_s	Density (g/cm^3)
0 05	0.90	10	0.50	5	1 80
0.5	1 75	30	1.00	15	1.80
2 0	4.90	100	2 80	50	2 40
14.0	5 20	4000	2.97	2000	2 60
30.0	6 00	4000	3.43	2000	2 90
Infinity	8.33	1000	4 83	500	3.30

et al.[9] for successfully modelling the Mexican M 8.1 earthquake suggest that this method may be reliably used for simulating the strong ground motion time histories for large earthquakes to provide a means for estimation of seismic hazard to guide the design of sensitive structures. In the next section we report on such an attempt for a M 8.5 gap filling earthquake in Garhwal Kumaon Himalaya.

Synthetic strong ground motion time histories at Tehri for a hypothetical M_w 8.5 earthquake

A simulation has been done to estimate the strong ground motions for a magnitude $M_w = 8.5$ earthquake located as shown in Figure 9. This models a 'seismic gap' filling earthquake in the future[17–19]. The fault plane is assumed to have the dimensions 80×240 km, its northern edge located at a depth of 18 km and dipping northward at 6°. The average slip is assumed to be 10 m, the shear modulus equal to 3×10^{11} dyne-cm^{-2}, and seismic moment about 6×10^{28}. The synthetics displayed in Figure 10 *a* are for stress drop of 50 and in Figure 10 *b* for 100 bars. We note that for the 1934

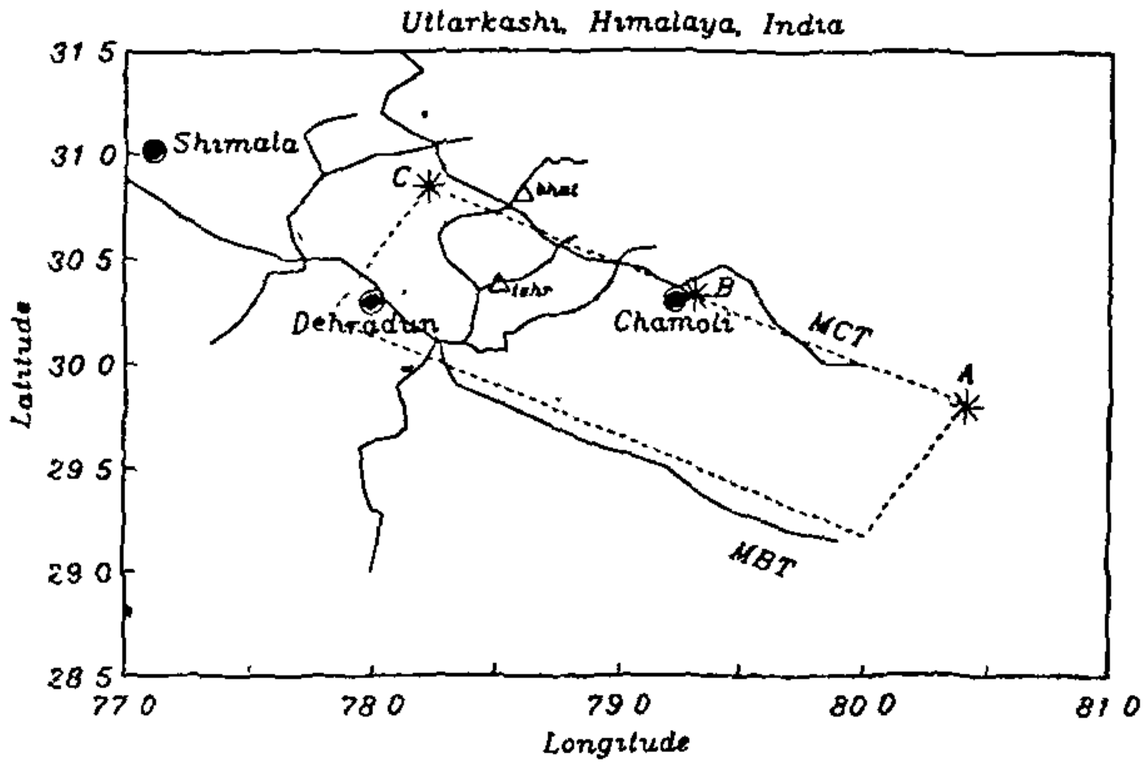

Figure 7. Pseudo-relative response spectra at Bhatwari. Long dash line: hypothetical M_w 8.5 earthquake; short dash line. synthetic for Uttarkashi earthquake (unfiltered); intermediate dash line: synthetic for Uttarkashi earthquake (filtered); solid line: observed for Uttarkashi earthquake (filtered). The *T* component has been analysed here. After Yu *et al* [14].

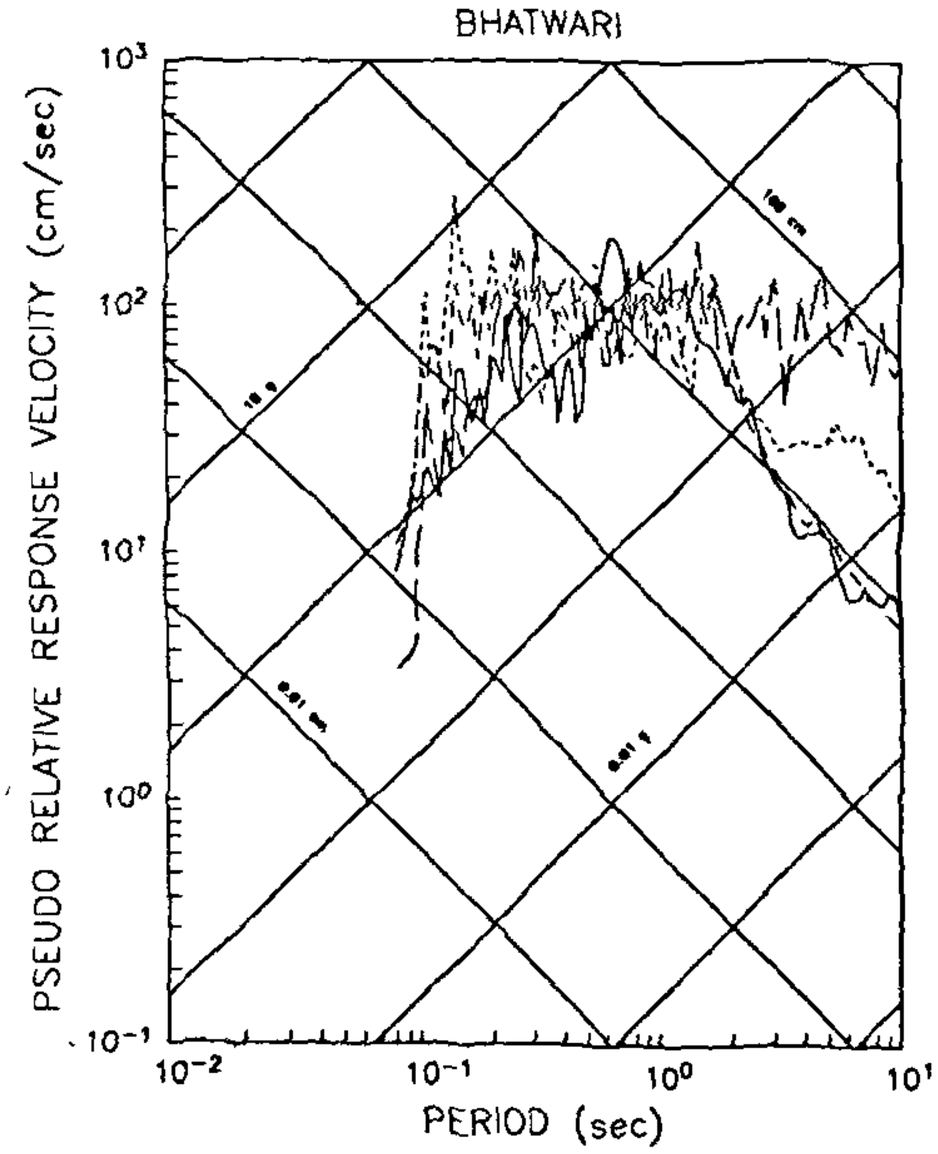

Figure 8. Pseudo-relative response spectra at Tehri. Details same as in Figure 7. After Yu *et al* [14].

great Bihar earthquake, Singh and Gupta[20] have estimated a stress drop of 275 bars, and for the 1935 Quetta earthquake 537 bars. Thus earthquakes in Himalaya can indeed have very large stress drops which influence the amplitudes of attendant strong ground motions. The peak accelerations for several impulses obtained in synthesized accelerograms are well above 50% g (0.5 g to 0.8 g) in the lower stress drop case and even greater than 100% g (1.2 g to 1.4 g) in the higher stress drop case. It is recognized that multiple simulations are needed to

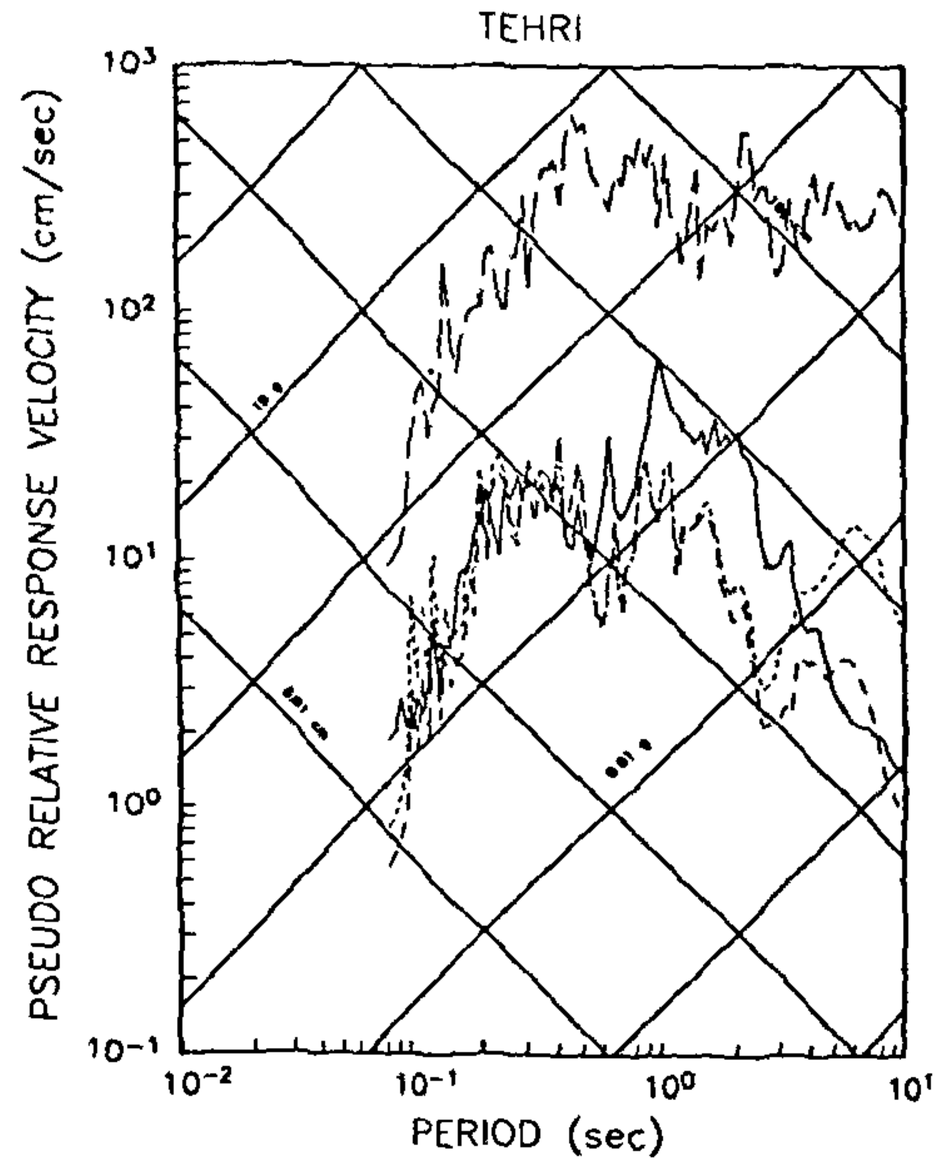

Figure 9. Location of a 'seismic gap' filling M_w = 8.5 earthquake in Garhwal-Kumaon Himalaya.

estimate variability of such synthetic accelerograms for a future earthquake. However, the example presented demonstrates the potential extent of peak accelerations which may be caused by a great earthquake. By employing a large number of simulations using a distribution of various critical parameters such as moment, stress drop, etc. as noted above a range of possible strong motion histories can be obtained to enable setting up percentile levels.

The response spectra for a hypothetical M_w 8.5 event are shown in Figures 7 and 8 by broken lines having higher amplitudes. The response spectra show considerably larger increase in acceleration amplitudes at lower frequencies as compared to that at higher frequencies, which is consistent with scaling laws of seismic spectrum.

Implications for seismic hazard

Although the synthetic strong ground motions for the M_w 8.5 earthquake have been calculated for a single realization of the faulting process, and it is recognized that variations in the source process of a future earthquake can occur in a number of ways which to some extent may influence the details of the resulting strong ground motion, the results of the above exercise appear to be relevant for making first-order estimates. One notices that in the period range of 1–2 s the pseudo-relative response acceleration amplitudes at Tehri for the hypothetical M_w 8.5 earthquake are in the neighbourhood of 1 g. At shorter periods the acceleration levels are even higher. This is the case for the stress drop of 50

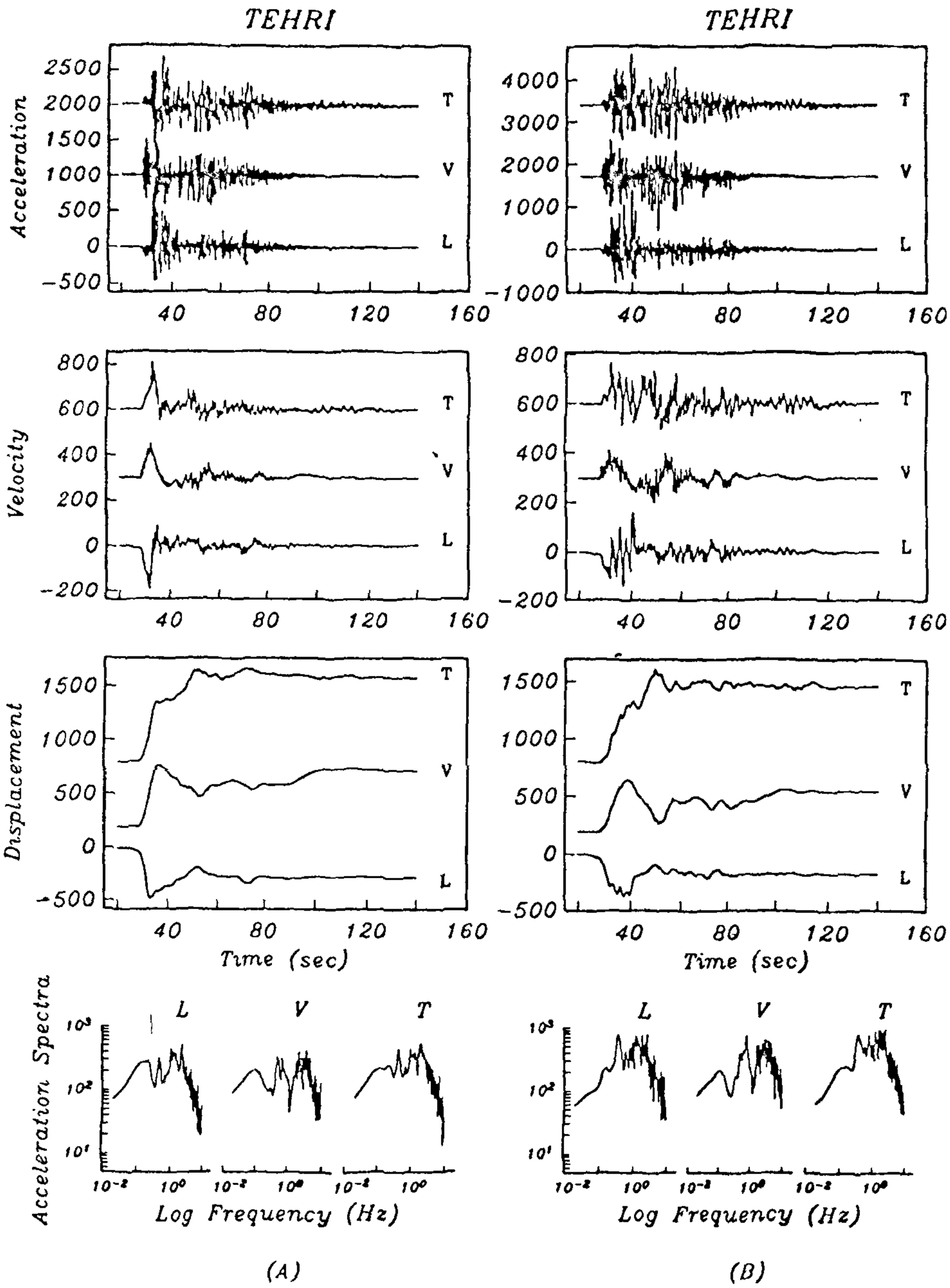

Figure 10. Synthetic acceleration, velocity, displacement time histories and Fourier spectra for acceleration at Tehri for a hypothetical M_w = 8.5 earthquake shown in Figure 7, having hypocentre *B* with (*a*) stress drop = 50 bars and (*b*) stress drop = 100 bars. After Yu *et al.*[14].

bars. For higher stress drop the accelerations will be even higher while if the stress drop was lower a corresponding decrease of accelerations can be anticipated. Furthermore, since the present technique has successfully modelled strong ground motions for the M_s 7.0 Uttarkashi earthquake as well as the M 8.1 Mexican earthquake, the estimate derived for a hypothetical M_w 8.5 earthquake is expected to reliably reflect the level of strong motions expected in the near field of a great earthquake in the Lesser Himalaya.

We recall that the fundamental period of the proposed Tehri dam in the Lesser Himalaya is variously estimated

between 1 and 2.272 s (ref. 21). The higher modes will have shorter periods. However, the value of acceleration in this period range adopted for the design of Tehri dam is only 0.22 g. It is thus apparent that the hazard figures adopted for the design of Tehri dam are significantly deficient in the light of results obtained from the present analysis.

Conclusions

This paper presents a method for modelling expected strong ground motion time histories using the composite fault model and synthetic Green's functions. It is shown that this flexible method is quite successful in modelling the Uttarkashi accelerograms and would be useful in estimating accelerograms for future earthquakes. Thus the method can be used to develop detailed and reliable estimates of seismic hazard for a safe design of critical structures in seismic areas.

1. Joyner, W. B. and Boore D. M, Proc. Earthquake Engg. & Soil Dynamics, Park City, Utah, Am. Soc. Civil Engrs., 1988, pp. 43–102.
2. Anderson, J. G., *Rev. Geophys., Seismol. Suppl*, U.S. National Report to the IUGG 1987–1990, pp. 700–720.
3. Aki, K. and Irikura, K., Proc. IV Int Conf. on Seismic Zonation, Earthquake Engg. Res Inst., Oakland, Calif., 1991, vol. 1, pp 61–110.
4. Brune, J N., *J. Geophys. Res.*, 1970, **75**, 4997–5009.
5. Brune, J N., *J. Geophys Res.*, 1971, **76**, 5002
6. Hartzell, S. H., *Geophys. Res. Lett.*, 1978, **5**, 104
7. Hutching, L. J. and Wu, F. T., *J. Geophys. Res.*, 1990, **95**, 1187–1224.
8. Aki, K. and Richards, P. G., *Quantitative Seismology: Theory and Methods*, W. H. Freeman and Co., New York, 1980.
9. Zeng, Y., Anderson, J. G. and Yu, G., A composite source model for computing realistic synthetic strong motions (submitted for publication), 1993.
10. Frankel, A., *J. Geophys. Res.*, 1991, **96**, 6291–6302.
11. Kanamori, H. and Anderson, D. L., *Bull. Seismol. Soc. Am.*, 1975, **65**, 1073–1096.
12. Luco, J. E. and Apsel, R. J, *Bull. Seismol. Soc. Am.*, 1983, **73**, 909–929.
13. Chandrasekaran, A. R. and Das, J. D., *Mem. Geol. Soc. India*, 1992, **23**, 81–122.
14. Yu, G., Khattri, K. N., Anderson, J. G., Brune, J. N and Zeng, Y., (submitted for publication), 1993.
15. Khattri, K N., *Mem. Geol. Soc. India*, 1992, **23**, 45–66.
16. Anooshehpoor, A. and Brune, J N., *Bull Seismol. Soc. Am*, 1989, **79**, 1247–1360.
17. Seeber, L. and Armbruster, J. G., in *Earthquake Prediction: An International Review*, Maurice Ewing Series, 4, Am. Geophys. Union, Washington DC, 1984, pp. 259–277.
18. Khattri, K. N., *Tectonophysics*, 1987, **138**, 79–92.
19. Molnar, P., *J. Him. Geol.*, 1990, **1**, 131.
20 Singh, D. D. and Gupta, H. K., *Bull. Seismol Soc. Am.*, 1984, **70**, 757–773
21. Iyenger, R. N., How Safe is Tehri Dam to Earthquakes, Workshop on 'Seismic Hazard and Large Dams in the Himalaya', Indian National Trust for Art and Cultural Heritage, New Delhi, 15–16 January, 1993.

ACKNOWLEDGEMENTS. KNK is indebted to CSIR and WIHG for support for this research and to Prof A. R. Chandrasekaran, UOR, and the DST for the release of the data.

Evaluation of design earthquake parameters for a site and utilization of strong motion data

A. R. Chandrasekaran
Department of Earthquake Engineering, University of Roorkee, Roorkee 247 667, India

A great majority of structures are designed according to provisions of the Code of Practice in respective countries. The so-called Site Dependent Evaluation of Earthquake Parameters are carried out for some important structural systems. In view of the stringent requirements of safety of nuclear power plants (NPP) very conservative procedures were developed for the prediction of earthquake parameters for design of NPP. Sometimes, the same techniques are sought to be applied for other structures where site-dependent studies are attempted. This paper discusses various aspects of this problem and suggests that prediction of maximum earthquake should not be based on which structure is supposed to be built in that area. One must leave to the judgement of the engineers to tone down the level of design earthquake from the maximum predicted earthquake depending on the methodology of design and acceptable level of damage. This paper also discusses utilization of results obtained from monitoring strong motion earthquakes.

Code provisions of various countries

MOST codes describe the seismicity in terms of seismic coefficient. It has been noted that there is a lot of misconception among scientists and engineers, to confuse seismic coefficient and peak ground acceleration. Seismic coefficient is generally related to response of short period structures (0.1 to 0.2 sec) to earthquakes and hence is larger than ground acceleration.

There are two broad philosophies followed in specifying seismic coefficient. In one, low values of seismic coefficients are specified, like that in Indian standards. However, simultaneously, the permissible increase in stresses due to these occasional loads is also kept small. In the second case, relatively large values are specified and simultaneously large increase in stresses is allowed.

The International Association for Earthquake Engineering (IAEE) brings out every four years a compilation of code of practice dealing with earthquake engineering